frontiers | Frontiers in Energy Research

TYPE Original Research
PUBLISHED 06 November 2024
DOI 10.3389/fenrg.2024.1478040

OPEN ACCESS

EDITED BY
Cong Zhang,
Hunan University, China

REVIEWED BY
Yang Liu,
South China University of Technology, China
Zhenjia Lin,
Hong Kong Polytechnic University, Hong Kong SAR, China

*CORRESPONDENCE
Jiajia Chen,
jjchen@sdut.edu.cn

RECEIVED 09 August 2024
ACCEPTED 01 October 2024
PUBLISHED 06 November 2024

CITATION
Li Y, Li K, Fan R, Chen J and Zhao Y (2024) Multi-objective planning of distribution network based on distributionally robust model predictive control.
Front. Energy Res. 12:1478040.
doi: 10.3389/fenrg.2024.1478040

Multi-objective planning of distribution network based on distributionally robust model predictive control

Yudun Li[1,2], Kuan Li[1,2], Rongqi Fan[3], Jiajia Chen[4]* and Yanlei Zhao[4]

[1]State Grid Shandong Electric Power Research Institute, Jinan, China, [2]State Grid Shandong Electric Power Company, Jinan, China, [3]Shandong Smart Grid Technology Innovation Center, Jinan, China, [4]Shandong University of Technology, Zibo, China

The uncoordinated integration of numerous distributed resources poses significant challenges to the safe and stable operation of distribution networks. To address the uncertainties associated with the intermittent output of distributed power sources, we propose a multi-objective planning strategy for distribution networks based on distributionally robust model predictive control (MPC). Initially, an error fuzzy set is established on a Wasserstein sphere using historical data to enhance out-of-sample performance. Next, a multi-objective optimization framework is constructed, balancing returns and risks, and is subsequently converted into a single-objective solution using value-at-risk conditions. This is followed by the implementation of multi-step rolling optimization within the model predictive control framework. We have linearized the proposed model using the linearized power flow method and conducted a thorough validation on an enhanced IEEE 37-node test system. Distributionally robust optimization (DRO) has been shown to reduce costs by a significant 29.16% when compared to an RO method. Moreover, the energy storage capacity required has been notably reduced by 33.33% on the 29-node system and by 20% on the 35-node system. These quantified results not only demonstrate the substantial economic efficiency gains but also the enhanced robustness of our proposed planning under the uncertainties associated with renewable energy integration.

KEYWORDS

distributionally robust optimization, model predictive control, uncertainty, distribution network planning, distributed resources

1 Introduction

With the advancement of new power system construction, distribution networks are evolving toward source-network-load-storage integration and collaborative interaction (Castro et al., 2024). The integration of large-scale distributed photovoltaic (PV) systems with uncertain output transforms distribution networks from radial passive structures into multi-power structures. This shift complicates power flow management and significantly impacts operational characteristics, leading to increased planning challenges (Zhang et al., 2023a; Esfahani et al., 2024). Addressing the capacity and scientific management of distributed power supplies and energy storage devices has thus become a research hotspot.

Many scholars have explored distribution network planning (Wang et al., 2024a; de Lima et al., 2024). For example, Pan et al. (2023) propose a collaborative planning method for distribution network and multi-energy systems, balancing multi-agent interests and improving analysis and calculation efficiency. Chen et al. (2017) introduce a multi-objective programming model based on game theory, considering the interests of source-grid-load multi-agents in a power market environment and using a particle swarm optimization algorithm for iterative optimization. Wang et al. (2022) propose a framework that considers energy storage allocation and bi-level planning of the distribution network, and the results show that this framework achieves low carbon emissions and improved economics. Subbaramaiah and Sujatha (2023) propose a multi-objective distribution network planning scheme that reduces power losses and identifies optimal wind power locations. However, these studies do not account for the impact of intermittent distributed PV output, potentially overestimating the system's risk resilience.

Scholars have increasingly recognized the pivotal role of energy storage in addressing the challenges of integrating high levels of renewable energy sources (Liu et al., 2023; Ma et al., 2024). For instance, Zheng et al. (2023) introduce an optimization framework for energy storage allocation in distribution networks with a significant penetration of photovoltaic (PV) systems. This approach addresses the source-load imbalance and voltage regulation issues, thereby reducing power losses and operational costs. Another notable contribution is made by Zhang et al. (2024), who present a method for the concurrent optimization of battery storage configuration and distribution network operations. The study demonstrates that energy storage can effectively smooth power fluctuations and enhance the network's resilience to fault disturbances. Through planning, the capacity of energy storage in the distribution network can increase the local consumption rate of renewable energy, reduce the system operating costs, and reduce the impact of PV uncertainty on the distribution network (Ba-swaimi et al., 2024; Li et al., 2024a). However, the above literature does not consider the risk assessment component in the energy storage configuration process.

Methods such as stochastic optimization, robust optimization, and distributionally robust optimization (DRO) are commonly used to address the uncertainty in high-proportion renewable energy predictions. Stochastic optimization assumes prediction errors follow specific probability distributions and uses manageable probability constraints (Wang et al., 2024b; Zhang et al., 2022; Li et al., 2024b). Robust optimization finds optimal solutions under worst-case scenarios, often resulting in overly conservative outcomes. DRO, on the other hand, uses real data to generate fuzzy sets and estimate distribution parameters, making it more suitable for complex, high-dimensional, multi-constraint problems (Skalyga et al., 2023). However, these constraints can turn the problem into a non-convex, nonlinear stochastic optimization challenge. Thus, a comprehensive approach that considers both economic benefits and operational safety is required. DRO focuses on establishing fuzzy sets with a flexible and diverse optimization framework. The Wasserstein distance, a measure of the difference between probability distributions, accurately describes similarities and differences by considering shape and weight information (Lu and Zhou, 2024).

Based on this analysis, the main contributions of this study are: (1) We consider energy storage capacity configuration and use a radius-controllable Wasserstein ball to construct a fuzzy set that achieves good out-of-sample performance, mitigating data overfitting and use distributed robust methods to balance robustness and economy. (2) Utilizing conditional value at risk (CVaR), we define optimization objectives for operation cost and constraint violation risk, transforming the multi-objective problem into a single-objective solution. (3) In order to reduce the error in PV forecasting, we implement rolling optimization within the model predictive control (MPC) framework.

2 Distributionally robust multi-objective model based on a Wasserstein sphere

2.1 Fuzzy set model based on a Wasserstein ball

Currently, there are two primary methods to model constraint distribution in distributionally robust optimization (DRO). One method involves moment-based fuzzy sets, such as unimodality (Zhang et al., 2021), symmetry (Wang et al., 2024c), and directional derivatives (Jiao et al., 2021), where fuzzy sets are defined as confidence intervals based on goodness-of-fit tests. The other method treats the fuzzy set as a ball in probability space, with the radius determined by metrics such as the Wasserstein metric, Kullback–Leibler divergence, and Prohorov metric.

Among these, the Wasserstein distance is particularly effective in measuring differences between two probability distributions. By considering both the shape and weight information of the distributions, it accurately captures the similarities and differences between them. In this paper, we construct fuzzy sets using the Wasserstein metric to achieve better out-of-sample performance and enhanced flexibility with radius control. Esfahani et al. (2024) demonstrated the effectiveness of data-driven Wasserstein metrics in solving distributed robust optimization re-representation problems. Inspired by this, our study employs the Wasserstein ball to construct fuzzy sets derived from limited prediction error data, thus achieving controllable data sets. Assuming the uncertainty set is a polyhedron, the prediction error ξ constitutes the data set $\Pi = \{\xi \in R^{N_\xi}: H\xi \le d_\xi\}$, as shown in Equation 1:

$$E^Q[\| \xi \|] = \int_\Pi \| \xi \| Q(d\xi) < \infty, \tag{1}$$

where $\| \cdot \|$ represents the norm, and $E^Q[\cdot]$ denotes the expectation operation under the Q distribution. The Wasserstein distance d_w is defined to represent the distance of all probability distributions Q of data set Π in space $m(\Pi)$. Let F be the set of all Lipschitz continuous functions f, and the constant is less than or equal to 1. The Wasserstein distance, as articulated by Equation 2, is a metric that grows with the number of samples, causing the fuzzy set to contract and ultimately converge to the true distribution. This convergence offers a more accurate and realistic portrayal of PV uncertainty (Skalyga et al., 2023). The Wasserstein distance

$\forall Q_1, Q_2 \in m(\Pi)$ between the empirical distribution d_w and the true distribution is calculated as follows:

$$d_w(Q_1, Q_2) = \max_{f \in F} \left[\begin{array}{l} \int_{\Pi} f(\xi) Q_1(d\xi) \\ -\int_{\Pi} f(\xi) Q_2(d\xi) \end{array} \right]. \tag{2}$$

The Wasserstein metric quantifies the minimum "distance" required to morph one probability distribution into another. The fuzzy set is delineated by encompassing all distributions within a controllable Wasserstein radius centered on the uniform empirical distribution derived from the training dataset, like Equation 3.

$$\hat{\mathbb{P}}^{N_s} = \left\{ Q \in m(\Pi) : d_w\left(\hat{P}^{N_s}, Q\right) \leq \gamma \right\}, \tag{3}$$

where $\hat{\mathbb{P}}^{N_s}$ contains all distributions $\hat{P}^{N_s}$ in a Wasserstein sphere with radius γ centered on the uniform empirical distribution. By adjusting the radius γ, the ball contains a true distribution P with a specified confidence level and good performance guarantee.

2.2 System optimization objective

The optimization goal of the system is to seek the balance between the operation cost and risk of the distribution network. Therefore, the objective function includes the sum of the operating cost function J_{cost} and the violation constraint risk function J_{risk}, namely Equation 4:

$$f = J_{\text{cost}} + J_{\text{risk}}. \tag{4}$$

1) The operating cost function J_{cost} is calculated as follows, as expressed in Equation 5:

$$J_{\text{cost}} = C_{\text{buy}} - C_{\text{sell}} + C_{\text{pre}} + C_{\text{cur}} + C_{\text{car}}, \tag{5}$$

where C_{buy}, C_{sell}, C_{pre}, C_{cur}, and C_{car} are electricity purchase cost, electricity sales income, operation, and maintenance cost, abandoned light cost, and carbon subsidy cost, respectively. The specific equations are expressed as Equations 6, 9 respectively

$$\begin{aligned} C_{\text{buy}} - C_{\text{sell}} = & \sum_{n \in N} a^t_{1,n} \left[P^t_{\text{l},n} + P^t_{\text{B},n} - (1 - \alpha^t_n) P^t_{\text{av},n} \right] \\ & + \sum_{n \in N} a^t_{2,n} \left[Q^t_{\text{l},n} - Q^t_{\text{av},n} \right] \\ & + \sum_{n \in N} a^t_{3,n} \left[(1 - \alpha^t_n) P^t_{\text{av},n} - P^t_{\text{l},n} - P^t_{\text{B},n} \right], \end{aligned} \tag{6}$$

where $P^t_{l,n}$ and $Q^t_{l,n}$ respectively represent the active and reactive power load of t bus $n \in N$ at the moment, $N = (1, 2, 3, \cdots, n)$ indicates the bus set, $P^t_{\text{av},n}$ and $Q^t_{\text{av},n}$ are the available active and reactive power generated by PV, respectively, and $P^t_{\text{B},n}$ denotes the charging and discharging power of the energy storage. The power reduction factor $\alpha^t_n \in [0, 1]$ is used to prevent the overvoltage hazard caused by high PV penetration. $a^t_{1,n}$ and $a^t_{2,n}$ represent the active and reactive power purchase prices, respectively, and $a^t_{3,n}$ refers to the active power sale price.

$$C_{\text{pre}} = \sum_{n \in N_{\text{av}}} a_{\text{av}} P^t_{\text{av},n} + \sum_{n \in N_{\text{B}}} a_{\text{B}} P^t_{\text{B},n}, \tag{7}$$

where $n \in N_{\text{av}}$ and $n \in N_{\text{B}}$ are the buses where the PV and energy storage are located, respectively; a_{av} and a_{B} are respectively the maintenance costs of unit power PV and energy storage.

$$C_{\text{cur}} = \sum_{n \in N_{\text{av}}} a^t_{4,n} \left[\alpha^t_n P^t_{\text{av},n} \right], \tag{8}$$

where $a^t_{4,n}$ represents the cost of discarding light.

$$C_{\text{car}} = \sum_{n \in N} a^t_{5,n} P^t_{\text{av},n}, \tag{9}$$

where $a^t_{5,n}$ denotes the government's carbon subsidy unit price for PV power generation.

2) The violation constraint risk function J_{risk} is computed as follows:

The risk function J_{risk} related to constraint violation encompasses the sum of the CVaR of the set of network and device constraint functions. This approach is supported by recent research in the field of energy systems and distribution network planning, as evidenced by Ren et al. (2024) and Chen et al. (2024). Specifically defined by Fan et al. (2023) and Zhang et al. (2023b), the CVaR measure is used to quantify the tail risk imposed by uncertainties, providing a more comprehensive assessment of risk than traditional measures

$$J^t_{\text{risk}} = \sum_{i=1}^{N_l} \text{CVaR}^{\beta}_{\mathbb{P}} \left[l_i(x_t, u_t, \xi_t) \right], \tag{10}$$

where N_l is the constraint set, and $\beta \in (0, 1]$ represents the CVaR confidence level of the random variable ξ_t under the $\mathbb{P}$ distribution. The specific details will be derived in the next section.

2.3 System constraints

2.3.1 PV output constraint

The distributed PV is connected to the distribution network through the inverter, and the relationship curve of the active and reactive power output characteristics is shown in Figure 1.

The relationship between the adjustable reactive power of the PV inverter on bus $n \in N$ and the inverter capacity $F_{\text{av},n}$ can be expressed as follows, namely Equation 11:

$$\sqrt{\left[(1 - \alpha^t_n) P^t_{\text{av},n} \right]^2 + \left(Q^t_{\text{av},n} \right)^2} \leq F_{\text{av},n}, \quad n \in N. \tag{11}$$

The reactive power output is limited by the power factor angle θ_n to be Equation 12

$$\left| Q^t_{\text{av},n} \right| \leq \tan(\theta_n) \left[(1 - \alpha^t_n) P^t_{\text{av},n} \right], \quad n \in N, \tag{12}$$

where the power factor angle θ_n of PV is also limited by $0 < \cos(\theta_n) \leq 1$.

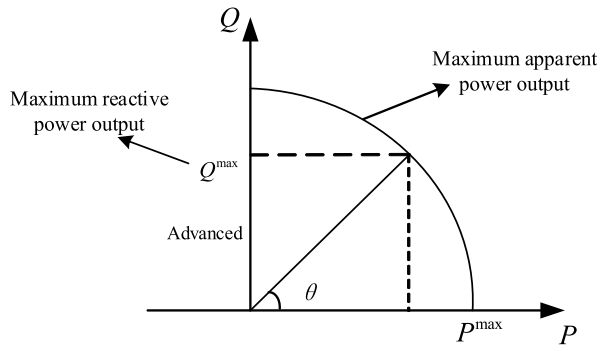

FIGURE 1
Distributed PV active and reactive power output characteristics.

2.3.2 Energy storage constraints

$$D_{es,n}^{t+1} = D_{es,n}^{t} + \eta_c P_{B_{c,n}}^{t} T - \frac{1}{\eta_d} P_{B_{d,n}}^{t} T, \quad n \in N, \tag{13}$$

where Equation 13 demonstrates the state-of-charge constraints for energy storage. T indicates the duration interval of $(t, t+1]$; $D_{es,n}^{t}$ denotes the state of charge of the energy storage device on the bus n; η_c and η_d are the charging and discharging efficiency, respectively. $P_{B_{c,n}}^{t}$ and $P_{B_{d,n}}^{t}$ represent the charging and discharging power stored at moment t, respectively. The charge/discharge power also satisfies $P_{B_{c,n}}^{t} P_{B_{d,n}}^{t} = 0$. The inequality constraints of energy storage capacity and power limit are Equation 14:

$$D_{es,n}^{min} \le D_{es,n}^{t} \le D_{es,n}^{max}, P_{B,n}^{min} \le P_{B,n}^{t} \le P_{B,n}^{max}, \tag{14}$$

where $D_{es,n}^{min}$ and $D_{es,n}^{max}$ are the minimum and maximum capacities of energy storage equipment, respectively; $P_{B,n}^{min}$ and $P_{B,n}^{max}$ represent respectively the impulse and discharge power limits.

2.3.3 Distribution network model

Suppose that the distribution network with N buses, $N = 1, 2, 3, \cdots, n$, $\boldsymbol{\Gamma} \subset N \times N$ represents the line connection matrix. Let $V_i^t \in C$ and $I_i^t \in C$ denote the voltage and current at node i at time t, $i \in N$, $\boldsymbol{V}^t = [V_1^t, V_2^t, \cdots, V_N^t]^T \in C^N$, and $\boldsymbol{I}^t = [I_1^t, I_2^t, \cdots, I_N^t]^T \in C^N$. Let $z_{ij} \in \boldsymbol{Z}$ represent the impedance between node i and node j, then the line admittance $y_{ij} = 1/z_{ij} = g_{ij} + jb_{ij}$, where $g_{ij} \in \boldsymbol{G}$ and $b_{ij} \in \boldsymbol{B}$ represent the conductance and susceptance between nodes, respectively. The bus bar is modeled using the Pi model, and the matrix y_{ij} of the admittance $\boldsymbol{Y}_{ij} \in C^{N \times N}$ can be expressed as Equation 15:

$$\boldsymbol{Y}_{ij} = \begin{cases} \sum_{l \sim i} y_{il} + y_{ii}, & i = j \\ -y_{ij}, & (i,j) \in \boldsymbol{\Gamma} \\ 0, & (i,j) \notin \boldsymbol{\Gamma}, \end{cases} \tag{15}$$

where $l \sim i$ means that the node i is connected to j. According to Kirchhoff's law and Ohm's law, $\boldsymbol{I}^t = \boldsymbol{Y}_{ij} \boldsymbol{V}^t$. Network complex power injection can be expressed as follows:

$$\boldsymbol{S}^t = \boldsymbol{V}^t (\boldsymbol{I}^t)^* = \mathrm{diag}(\boldsymbol{V}^t)(\boldsymbol{Y}\boldsymbol{V}^t)^*, \tag{16}$$

where the superscript "*" represents the conjugate operation, and the complex power $\boldsymbol{S}^t = [S_1^t, S_2^t, \cdots, S_N^t]^T$ can be decomposed into $S_i^t = P_i^t + jQ_i^t$ in the rectangular coordinate, where P_i^t and Q_i^t represent the active power and reactive power injected by the node, respectively.

3 Multi-objective planning based on DROMPC

3.1 Dynamic characteristics with MPC

Consider N_d grid-connected devices, including a traditional generator, an inverter-based distributed power supply, and time-varying load. Energy storage devices, such as batteries and plug-in electric vehicles, can be used both as generators and as loads. The power flow of each controllable device is modeled by a discrete linear dynamic system as follows Equation 17:

$$x_{t+1}^d = \bar{A}^d x_t^d + \bar{B}^d u_t^d, \tag{17}$$

where the state variable $x_t^d \in R^{n_d}$ of the device d at the time t, the dynamic matrix $\bar{A}^d \in R^{n_d \times n_d}$, and the coefficient input matrix $\bar{B}^d \in R^{n_d \times m_d}$ of the control variable $u_t^d \in R^{m_d}$. The first element of x_t^d corresponds to the output power of device d to the distribution network at t time.

Let the control domain be H; then, the matrix form of system evolution can be expressed as Equation 18:

$$\boldsymbol{x}_t^d = \boldsymbol{A}_t^d x_0^d + \boldsymbol{B}_t^d \boldsymbol{u}_t^d, \tag{18}$$

where $\boldsymbol{x}_t^d$ is the state vector, $\boldsymbol{x}_t^d = [x_1^d, x_2^d, \cdots, x_t^d]^\top$ contains all the state variables in the control domain; $\boldsymbol{u}_t^d$ denotes the control matrix, and $\boldsymbol{u}_t^d = [u_0^d, u_1^d, \cdots, u_{t-1}^d]^\top$. The calculation formulas of $\boldsymbol{A}_t^d$ and $\boldsymbol{B}_t^d$ can be expressed as Equation 19:

$$\boldsymbol{A}_t^d = \begin{bmatrix} \bar{A}^d \\ \left(\bar{A}^d\right)^2 \\ \vdots \\ \left(\bar{A}^d\right)^t \end{bmatrix}, \boldsymbol{B}_t^d = \begin{bmatrix} \bar{B}^d & 0 & \cdots & 0 \\ \bar{A}^d \bar{B}^d & \bar{B}^d & \cdots & 0 \\ \vdots & \vdots & \vdots & \vdots \\ \left(\bar{A}^d\right)^{t-1} \bar{B}^d & \cdots & \bar{A}^d \bar{B}^d & \bar{B}^d \end{bmatrix}. \tag{19}$$

3.2 Linearized approximate power flow

In this paper, the linearization method of literature (Alizadeh and Capitanescu, 2022) is used to linearize the power flow model shown in Equation 16. In a balanced, symmetrical distribution network, the common coupling point connected to the power grid is denoted as node 0, serving as the bus set that connects the load and the distributed generator.

The complex form of the node voltage is $V_n^t = |V_n^t| e^{j \angle V_n^t}$, and the node injection current is expressed as $I_n^t = |I_n^t| e^{j \angle I_n^t}$, where $|V_n^t|$ and $|I_n^t|$ correspond to the root mean square value, and $\angle V_n^t$ and $\angle I_n^t$ are the relative phase angles of voltage and current, respectively. The node 0 denotes the slack node, and the other nodes are the PQ nodes that inject complex power. The admittance matrix can be divided into

10.3389/fenrg.2024.1478040

$$\begin{bmatrix} I_0^t \\ \boldsymbol{I}^t \end{bmatrix} = \begin{bmatrix} y_{00} & \bar{y}^{\top} \\ \bar{y} & \boldsymbol{Y} \end{bmatrix} \begin{bmatrix} V_0 \\ \boldsymbol{V}^t \end{bmatrix}, \tag{20}$$

where V_0 is the slack bus voltage; I_0^t is the current injected into the slack bus at time t; y_{00} is the self-admittance of the slack node; $\bar{y}$ indicates transfer admittance.

The injection power presented in Equation 20 can be formulated as follows:

$$\boldsymbol{S}^t = \mathrm{diag}(\boldsymbol{V}^t)(\boldsymbol{Y}^{\star}(\boldsymbol{V}^t)^{\star} + \bar{y}^{\star}(V_0^t)^{\star}). \tag{21}$$

Assuming that $\bar{\boldsymbol{V}} = |\bar{V}|\angle\boldsymbol{\theta}$ is a preset nominal voltage value, and ΔV^t represents the difference between the actual voltage and the nominal voltage, the voltage can be expressed as $\boldsymbol{V}^t = \bar{\boldsymbol{V}} + \Delta\boldsymbol{V}^t$. Then, Equation 21 becomes Equation 22:

$$\boldsymbol{S}^t = \mathrm{diag}(\bar{\boldsymbol{V}} + \Delta\boldsymbol{V}^t)(\boldsymbol{Y}^{\star}(\bar{\boldsymbol{V}} + \Delta\boldsymbol{V}^t)^{\star} + \bar{y}^{\star}V_0^{*}). \tag{22}$$

Ignoring the influence of the higher-order term $\mathrm{diag}(\Delta\boldsymbol{V}^t)\boldsymbol{Y}^{\star}(\Delta\boldsymbol{V}^t)^{\star}$, the power constraint equation is transformed into Equation 23:

$$\Lambda\Delta\boldsymbol{V}^t + \Phi(\Delta\boldsymbol{V}^t)^{\star} = \boldsymbol{S}^t + \Psi, \tag{23}$$

where

$\Lambda = \mathrm{diag}(\boldsymbol{Y}^{\star}\bar{\boldsymbol{V}}^{\star} + \bar{y}^{\star}V_0^{*})$;

$\Phi = \mathrm{diag}(\bar{\boldsymbol{V}})\boldsymbol{Y}^{\star}, \Psi = -\mathrm{diag}(\bar{\boldsymbol{V}})(\boldsymbol{Y}^{\star}\bar{\boldsymbol{V}}^{\star} + \bar{y}^{\star}V_0^{*})$。

Given $\Lambda = 0_{N\times N}$ and $\psi = 0_N$, the nominal voltage is $\bar{\boldsymbol{V}} = \boldsymbol{Y}^{-1}\bar{y}V_0$, and the linearized power is expressed as $\boldsymbol{S}^t = \mathrm{diag}(\bar{\boldsymbol{V}})\boldsymbol{Y}^{\star}(\Delta\boldsymbol{V}^t)^{\star}$. The voltage deviation becomes Equation 24:

$$\Delta\boldsymbol{V}^t = \boldsymbol{Y}^{-1}\mathrm{diag}^{-1}(\bar{\boldsymbol{V}}^{\star})(\boldsymbol{S}^t)^{\star}. \tag{24}$$

Let $\boldsymbol{Z}_R$ be the real part of the impedance and $\boldsymbol{Z}_I$ be the imaginary part of the impedance, then $\boldsymbol{Y}^{-1} = (\boldsymbol{G} + j\boldsymbol{B})^{-1} = \boldsymbol{Z}_R + j\boldsymbol{Z}_I$. Taking M and N as the active and reactive component coefficients, respectively, $\Delta\boldsymbol{V}^t$ is expanded in the form of rectangular coordinates as Equation 25:

$$\begin{aligned} M &= \left(\boldsymbol{Z}_R\mathrm{diag}\left(\frac{\cos(\theta)}{|\bar{\boldsymbol{V}}|}\right) - \boldsymbol{Z}_I\mathrm{diag}\left(\frac{\sin(\theta)}{|\bar{\boldsymbol{V}}|}\right)\right), \\ N &= \left(\boldsymbol{Z}_I\mathrm{diag}\left(\frac{\cos(\theta)}{|\bar{\boldsymbol{V}}|}\right) - \boldsymbol{Z}_R\mathrm{diag}\left(\frac{\sin(\theta)}{|\bar{\boldsymbol{V}}|}\right)\right). \end{aligned} \tag{25}$$

The voltage amplitude is approximately equal to $|\bar{\boldsymbol{V}}| + R(\Delta\boldsymbol{V}^t)$, $R(\cdot)$ represents the real part operation, and $\mathbb{I}$ indicates the unit matrix. Referring to the linear relationship between voltage and power, the voltage amplitude is finally expressed as Equation 26:

$$\boldsymbol{V}^{\mathrm{t}}[p^t, q^t] = M(\mathbb{I} - \mathrm{diag}\{\alpha_n^t\})P_{\mathrm{av},n}^t + NQ^t + |\bar{\boldsymbol{V}}|. \tag{26}$$

The voltage constraint is shown in Equation 27:

$$\boldsymbol{V}^{\mathrm{t}}[p^t, q^t] - \boldsymbol{V}^{\max} \le 0, \boldsymbol{V}^{\min} - \boldsymbol{V}^{\mathrm{t}}[p^t, q^t] \le 0, \tag{27}$$

where $\boldsymbol{V}^{\min}$ and $\boldsymbol{V}^{\max}$ are the matrix forms of the lower limit $V^{\min}$ and the upper limit $V^{\max}$ of the line voltage, respectively.

3.3 DROMPC for distribution network planning

In this paper, the device constraints and voltage constraints under different times and nodes can be summarized as follows:

$$\begin{cases} E\boldsymbol{\mathcal{R}}[\boldsymbol{V}^{\mathrm{t}}[p^t, q^t] - \boldsymbol{V}^{\max} \le 0] \\ E\boldsymbol{\mathcal{R}}[\boldsymbol{V}^{\min} - \boldsymbol{V}^{\mathrm{t}}[p^t, q^t] \le 0] \\ E\boldsymbol{\mathcal{R}}[\mathbf{T}_d^t\boldsymbol{x}_t^d + \mathbf{U}_d^t\boldsymbol{u}_t^d + \mathbf{Z}_d^t\boldsymbol{\xi}_t - \omega_d \le 0], \end{cases} \tag{28}$$

where $\boldsymbol{\mathcal{R}}[\cdot]$ denotes the general transformation from inequality constraints to random form. $\mathbf{T}_d^t\boldsymbol{x}_t^d + \mathbf{U}_d^t\boldsymbol{u}_t^d + \mathbf{Z}_d^t\boldsymbol{\xi}_t - \omega_d \le 0$ contains various local constraints of grid-connected equipment; $\mathbf{T}_d^t$, $\mathbf{U}_d^t$, and $\mathbf{Z}_d^t$ are the coefficient matrices of equipment state variables, control variables, and uncertain errors, respectively. ω_d is a local constraint parameter. In this paper, CVaR is used to re-describe the voltage affine constraints, and the remaining constraints are evaluated by sample average.

Define an affine constraint set $\boldsymbol{\mathcal{V}}_t$ containing N_l Equation 28, where each affine constraint can be expressed as Equation 29:

$$\mathcal{C}_o^t(\mathbf{y}_t, \xi_t) = \left[\bar{\mathcal{A}}(\mathbf{y}_t)\right]_o\xi_t + \left[\bar{\mathcal{B}}(\mathbf{y}_t)\right]_o, \tag{29}$$

where $\mathcal{C}_o^t(\cdot)$ is the $o, o = 1, \cdots, N_l$ affine constraint in $\boldsymbol{\mathcal{V}}_t$. The decision variable $\mathbf{y}_t$ includes the PV reduction variable α_n^t and the controllable device setting point. The CVaR constrained at confidence level β in A $\boldsymbol{\mathcal{V}}_t$ is calculated as follows Equation 30:

$$\inf_{\kappa_o^t} E_{\xi_t}\left\{\left[\mathcal{C}_o^t(\mathbf{y}_t, \xi_t) + \kappa_o^t\right]_+ - \kappa_o^t\beta\right\} \le 0, \tag{30}$$

where κ_o^t is an auxiliary variable. The expected operation in the above equation can be restated as Equation 31:

$$\bar{\mathcal{Q}}_o^t = \max_{k=1,2}[\langle\bar{\mathbf{a}}_{ok}(\mathbf{y}_t), \xi_t\rangle + \bar{\mathbf{b}}_{ok}(\kappa_o^t)]. \tag{31}$$

Because the result is the maximum of two affine functions, the expression is convex in $\mathbf{y}_t$ for each fixed ξ_t. The risk objective shown in Equation 10 is expressed by the distributionally robust optimization form of CVaR as follows Equation 32:

$$\hat{J}_{\mathrm{risk}}^t = \sum_{t=1}^{H}\sum_{o=1}^{N_l}\sup_{Q_t\in\hat{\mathbb{P}}_t^{N_s}} E^{Q_t}\max_{k=1,2}\left[\langle\bar{\mathbf{a}}_{ok}(\mathbf{y}_t), \hat{\xi}_t\rangle + \bar{\mathbf{b}}_{ok}(\kappa_o^t)\right]. \tag{32}$$

The above multi-objective DRO is equivalently restated as a single-objective quadratic programming using the method of Lin et al. (2023). The objective is to minimize the total worst-case CVaR of the function and affine constraints. The specific form of the subproblem of MPC is as follows Equation 33:

$$\begin{aligned} &\left\{\inf_{\substack{\omega_{1,n},\omega_{2,n},\\ \mathbf{y}_t,\kappa_o^t}}\sum_{t=1}^{H}\left\{\mathrm{E}\left[\hat{J}_{\mathrm{cost}}^t\right] + \sup_{Q_t\in\hat{\mathbb{P}}_t^{N_s}}\sum_{o=1}^{N_l}\mathrm{E}^{Q_t}\left[\bar{\mathcal{Q}}_o^t\right]\right\}\right. \\ &\quad = \inf_{\substack{\omega_{1,n},\omega_{2,n},\\ \mathbf{y}_t,\kappa_o^t,\\ \lambda_o,s_{io}^t,\varsigma_{iko}^t}}\sum_{t=1}^{H}\left\{\mathrm{E}\left[\hat{J}_{\mathrm{cost}}^t\right] + \sum_{o=1}^{N_l}\left(\lambda_o\gamma_t + \frac{1}{N_s}\sum_{i=1}^{N_s}s_{io}^t\right)\right\} \\ &\quad \text{s.t.} \quad (\bar{\mathbf{b}}_{ok}(\kappa_o^t) + \langle\bar{\mathbf{a}}_{ok}(\mathbf{y}_t), \hat{\xi}_t^i\rangle \le s_{io}^t \parallel \varsigma_{iko}^t \end{aligned}$$

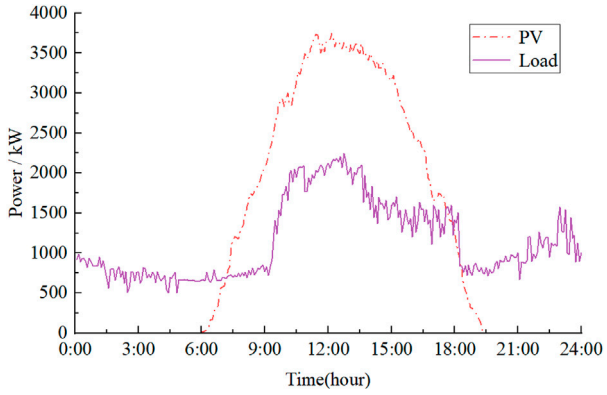

FIGURE 2
Curves of available PV power and total load demand.

$$-\bar{\mathbf{a}}_{ok}(\mathbf{y}_t)\|_{\infty} \le \lambda_o^t \varsigma_{iko}^t \ge 0 \frac{1}{N_s}\sum_{i=1}^{N_s}\left[\left[(1-\alpha_n^t)\hat{P}_{\mathrm{av},n}^{t,i}\right]^2\right.$$

$$+(Q_n^t)^2 - \bar{S}_n^2 + \varpi_{1,n}^t]_+ \le \varpi_{1,n}^t \beta \frac{1}{N_s}\sum_{i=1}^{N_s}\left[\tan(\theta_n)\left[(1-\alpha_n^t)\hat{P}_{\mathrm{av},n}^{t,i}\right]\right.$$

$$-|Q_n^t| + \varpi_{2,n}^t]_+ \le \varpi_{2,n}^t \beta$$

Equations (13) − (14), (33)

where $\varpi_{1,n}^t$, $\varpi_{2,n}^t$, and κ_o^t are auxiliary variables of CVaR, λ_o^t, s_{io}^t, and ς_{iko}^t are auxiliary variables of distributionally robust Wasserstein sphere reconstruction (Dong et al. (2024)). The power factor constraint and apparent power constraint are processed by sample average.

4 Simulation and discussion

4.1 System description and parameter settings

To verify the effectiveness of the proposed optimization framework, we conducted simulations using the improved IEEE 37-bus system, with network parameters derived from Reference Chen et al. (2023). The modified network is a single-phase equivalent network, as shown in Figure 2, and includes 21 PV inverters. Table 1 lists their positions and capacities. Figure 3 displays the total available PV power and total load demand throughout the day. The energy storage charge and discharge efficiency are set at 90%.

In this verification case, the upper and lower limits of voltage optimization are set to $V^{\min} = 0.95$ p.u. and $V^{\max} = 1.05$ p.u., respectively. The power factor is set to 0.9. The optimization decision interval is set to 5 min. The remaining parameters are shown in Table 2. Aiming at the difficulty and complexity of solving the distributed robust optimization problem, the cvx convex optimization toolbox is called in MATLAB for calculation.

4.2 Simulation results

Table 3 now includes a comprehensive comparison of energy storage planning results using the DRO-based MPC method proposed in this paper, along with the RO and SO methods for the 29th and 35th nodes. The table provides specific numerical values for the energy storage configurations obtained through each method. Table 4 presents a detailed comparison of operating costs under various strategic planning methods. The table now includes exact figures for the maximum, mean, and standard deviation of total operating costs for each method.

The quantified results, as shown in Table 3, indicate that the use of the DRO method leads to a 29.16% reduction in cost compared to the RO method, with energy storage capacities reduced by 33.33% and 20% on the 29- and 35-node systems, respectively. Furthermore, Table 4 reveals that the DRO method achieves maximum, mean, and standard deviation values of total operating costs that are 12.5%, 0.75%, and 51.3% lower than those obtained using the RO method, respectively.

These improvements are attributed to the DRO method's ability to utilize real data, offering more flexible and reliable planning support. This approach avoids the excessive conservatism and economic sacrifices associated with the RO method, which adopts a worst-case distribution strategy, and the SO method, which, despite using a preset probability distribution for energy storage capacity configuration, lacks adaptability in actual scheduling.

The SO, RO, and DRO methods are used for optimization under the same planning scheme. Figure 4 shows the system operation cost

TABLE 1 Location and capacity of PV and energy storage.

Node	PV(kW)/ES(kWh)	Node	PV(kW)/ES(kWh)	Node	PV(kW)/ES(kWh)
4	150/-	17	360/-	30	360/-
7	300/-	20	450/-	31	500/-
9	300/100	22	150/-	32	330/250
10	600/100	23	500/-	33	500/-
11	660/-	26	300/-	34	450/-
13	360/-	28	500/50	35	450/-
16	600/-	29	300/-	36	450/200

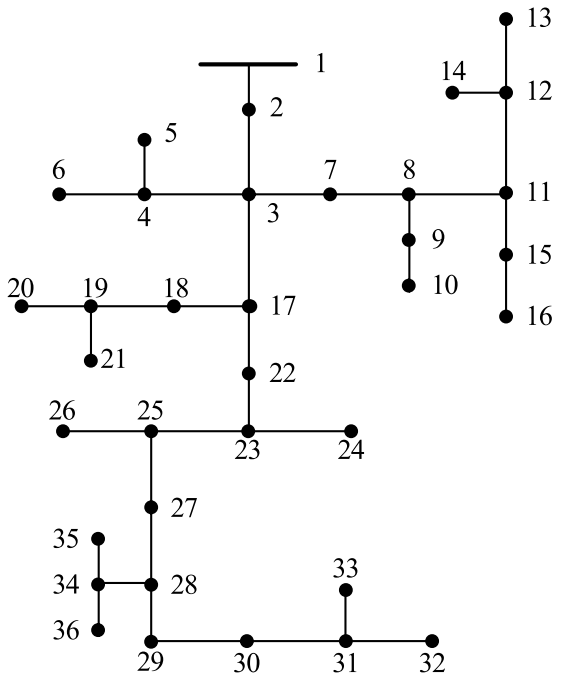

FIGURE 3
Improved IEEE 37-node test system.

from 10:00 to 15:00 for each method. Table 3 presents the maximum, minimum, average, and standard deviation of the system operation costs under these different methods. The results indicate that the proposed method outperforms the traditional RO method in terms of operation cost and demonstrates better economic efficiency. Although the proposed method is less economical than the SO method, it has a smaller skewness, leading to smoother system operation under uncertainty.

Figure 5 shows the operating voltages under the three planning strategies. It is evident that under the SO method, high uncertainty impacts lead to voltage limit violations due to excessive emphasis on economic factors, significantly reducing system robustness. The proposed method considers worst-case planning results by solving the distribution cluster containing the empirical distribution, aligning better with the modeling of uncertain outputs from different renewable energy sources, and thus offers stronger robustness than traditional stochastic optimization.

In summary, the DRO-based MPC method proposed in this paper effectively balances the relationship between economic efficiency and robustness. The proposed planning comprehensively addresses the probability of prediction errors. The average reduction in PV power achieved with this strategy is 645.510 kW, providing an effective control approach for managing significant deviations in PV predictions. Although ensuring voltage security and stability, the proposed strategy increases the average power reduction by 36.851%, thereby enhancing the distribution network's robustness in handling the uncertainties associated with renewable energy predictions.

Table 5 presents a comparative analysis of system costs and PV consumption rates under two scenarios for the IEEE 37-node system. "Case 1" includes energy storage configuration, while "Case 2" does not. The data clearly show that including energy

TABLE 2 System parameters

Parameter	Value	Parameter	Value	Parameter	Value
$a^t_{1,n}$	0.6 CNY/kW	$a^t_{4,n}$	0.6 CNY/kW	a_B	0.04 CNY/kW
$a^t_{2,n}$	0.6 CNY/kW	$a^t_{5,n}$	0.2 CNY/kW	β	0.01
$a^t_{3,n}$	0.4 CNY/kW	a_{av}	0.06 CNY/kW		

TABLE 3 Energy storage configuration under different strategic planning schemes.

Method	29-Node	35-Node	Cost/10^4CNY
RO	300 kWh	150 kWh	48
SO	150 kWh	80 kWh	26
DRO	200 kWh	120 kWh	34

TABLE 4 Comparison of operating costs under different strategic planning schemes.

Method	Total operating cost/10^4CNY			
	Minimum value	Maximum value	Mean value	Standard deviation
RO	76.26	110.73	92.08	7.60
SO	72.21	91.35	80.96	4.04
DRO	79.28	96.91	85.16	3.70

10.3389/fenrg.2024.1478040

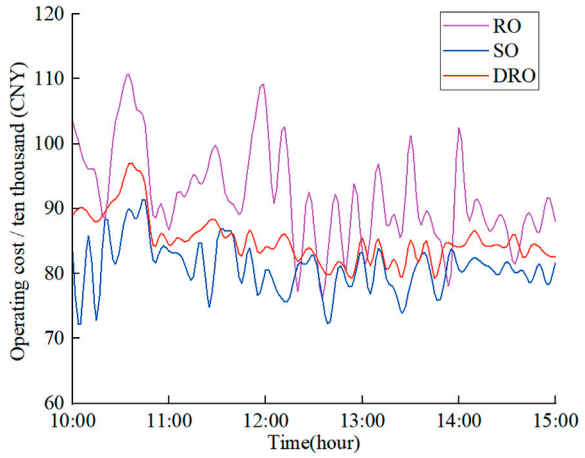

FIGURE 4
Operating costs under different strategic planning.

storage leads to a 2.85% reduction in system cost and a 1.2% increase in the PV in-situ consumption rate.

Figure 6A illustrates the purchased and sold power from the substation for the IEEE 37-node system. Figure 6B depicts the charging and discharging patterns of the energy storage system. These figures demonstrate how excess PV output is stored during periods of low demand and utilized during high demand, effectively performing peak-shaving and load-balancing functions that enhance the economic efficiency and reliability of the distribution network.

4.3 The influence of different Wasserstein spheres

To illustrate the impact of the Wasserstein sphere radius on planning results, various radius values are used to compare the total operational costs. As shown in Table 6, increasing the radius of the Wasserstein sphere results in a broader coverage of uncertainties by the fuzzy set. This broader coverage leads to more conservative decision-making, which in turn raises operating costs but results in a smoother operational mode. Consequently, the proposed method allows for more flexible control of robustness and economic efficiency by adjusting the radius of the Wasserstein sphere.

5 Conclusion

This paper introduces a multi-objective planning approach for DRO power systems utilizing MPC to tackle the uncertainty challenges posed by high levels of renewable energy integration in distribution networks. The proposed method offers a flexible balance between economic efficiency and operational robustness. The key quantitative conclusions drawn from our analysis are:

(1) The DRO-MPC approach significantly mitigates the impact of uncertainty from large-scale distributed PV output on

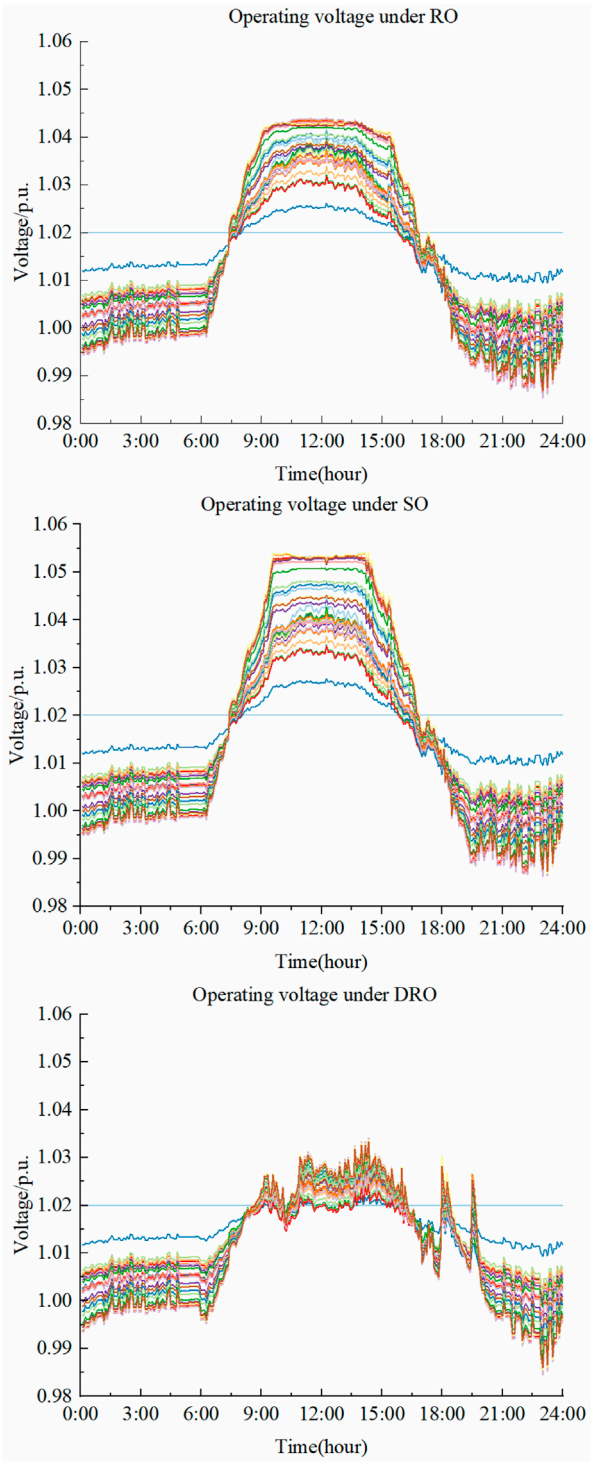

FIGURE 5
Operating voltage under different strategic planning.

TABLE 5 Results of total operating cost and PV consumption rate on the IEEE 37-node system.

	Total operating cost/ 104CNY	Local consumption rate/%
Case 1	34	98.48
Case 2	35	97.31

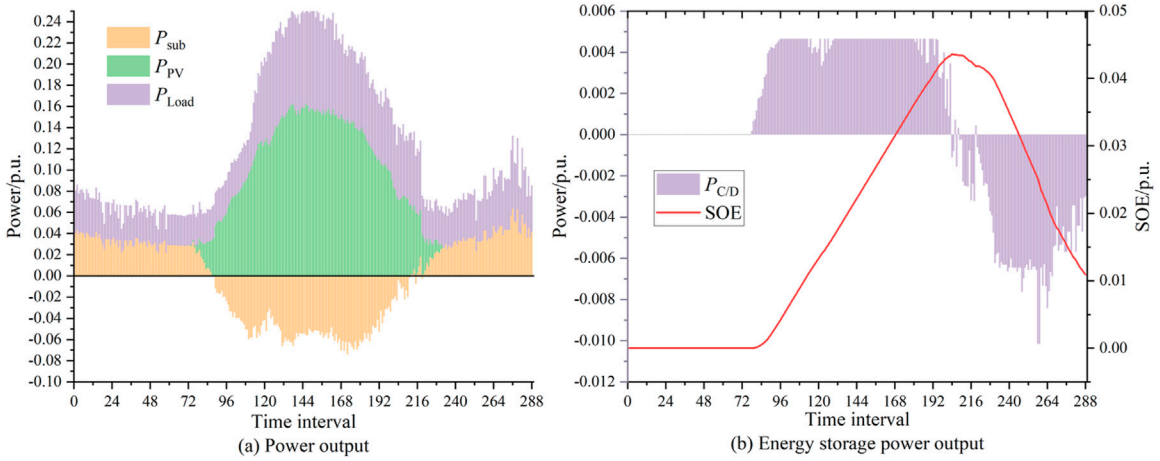

FIGURE 6
Optimal operation results of the IEEE 37-inode system.

TABLE 6 Impact of different Wasserstein sphere radii on planning results.

γ	Total operating cost/10^4CNY			
	Minimum value	Maximum value	Mean value	Standard deviation
0	78.76	96.63	84.84	3.76
0.001	79.28	96.91	85.16	3.70
0.002	79.68	97.58	85.92	3.57

distribution network planning. It enhances economic efficiency and maintains system robustness, reducing costs by 29.16% compared to the RO method. Additionally, the energy storage capacity is optimized, resulting in a 33.33% reduction on the 29-node system and a 20% reduction on the 35-node system.

(2) By transforming the computationally intensive multi-objective problem into a streamlined single-objective solution, our method overcomes the limitations inherent in traditional multi-objective optimization approaches.

(3) The planning scheme's adaptability is further enhanced by the variable radius of the Wasserstein sphere, allowing for greater flexibility and tailored responses to different operational scenarios.

Data availability statement

The original contributions presented in the study are included in the article/supplementary material; further inquiries can be directed to the corresponding author.

Author contributions

YL: conceptualization, funding acquisition, and writing–original draft. KL: investigation, methodology, and writing–original draft. RF: investigation, methodology, and writing–original draft. JC: conceptualization, supervision, and writing–review and editing. YZ: supervision and writing–review and editing.

Funding

The author(s) declare that financial support was received for the research, authorship, and/or publication of this article.

Conflict of interest

Authors YL and KL, were employed by State Grid Shandong Electric Power Research Institute and State Grid Shandong Electric Power Company.

The remaining authors declare that the research was conducted in the absence of any commercial or financial relationships that could be construed as a potential conflict of interest.

The authors declare that this study received funding from the State Grid Shandong Electric Power Company Technology Project on Renewable Energy Dominated Regional Power Grid Islanding Mechanism and High Reliability Control and Protection Technology (No. 52062623S034). The funder had the following involvement in the study: design, collection, analysis, interpretation of data, and the writing of this article.

Publisher's note

References

Alizadeh, M. I., and Capitanescu, F. (2022). A tractable linearization-based approximated solution methodology to stochastic multi-period AC security-constrained optimal power flow. *IEEE Trans. Power Syst.* 38 (6), 5896–5908. doi:10.1109/tpwrs.2022.3220283

Ba-swaimi, S., Verayiah, R., Ramachandaramurthy, V. K., and Alahmad, A. K. (2024). Long-term optimal planning of distributed generations and battery energy storage systems towards high integration of green energy considering uncertainty and demand response program. *J. Energy Storage* 100, 113562. doi:10.1016/j.est.2024.113562

Castro, F., Canizes, B., Soares, J., Almeida, J., and Vale, Z. (2024). Comprehensive framework for distribution network multi-investment expansion planning: emissions, uncertainty, and resource remuneration integration. *Energy Convers. Manag.* 316, 118734. doi:10.1016/j.enconman.2024.118734

Chen, H., Gao, P., Liu, K., Chen, L., and Huang, W. (2024). Joint expansion planning for data centers and distribution networks based on conditional value-at-risk theory considering low carbon characteristics. *Electr. Power Syst. Res.* 229, 110162. doi:10.1016/j.epsr.2024.110162

Chen, J., Zheng, J., Wu, P., Zhang, L., and Wu, Q. (2017). Dynamic particle swarm optimizer with escaping prey for solving constrained non-convex and piecewise optimization problems. *Expert Syst. Appl.* 86, 208–223. doi:10.1016/j.eswa.2017.05.047

Chen, Y., Jacob, R. A., Gel, Y. R., Zhang, J., and Poor, H. V. (2023). Learning power grid outages with higher-order topological neural networks. *IEEE Trans. Power Syst.* 39 (1), 720–732. doi:10.1109/tpwrs.2023.3266956

de Lima, T. D., Lezama, F., Soares, J., Franco, J. F., and Vale, Z. (2024). Modern distribution system expansion planning considering new market designs: review and future directions. *Renew. Sustain. Energy Rev.* 202, 114709. doi:10.1016/j.rser.2024.114709

Dong, G., Zhu, Z., Lou, Y., Yu, J., Wu, L., and Wei, J. (2024). Optimal charging of lithium-ion battery using distributionally robust model predictive control with Wasserstein metric. *IEEE Trans. Industrial Inf.* 20 (5), 7630–7640. doi:10.1109/tii.2024.3363079

Esfahani, M., Alizadeh, A., Amjady, N., and Kamwa, I. (2024). A distributed VPP-integrated co-optimization framework for energy scheduling, frequency regulation, and voltage support using data-driven distributionally robust optimization with Wasserstein metric. *Appl. Energy* 361, 122883. doi:10.1016/j.apenergy.2024.122883

Fan, W., Tan, Z., Li, F., Zhang, A., Ju, L., Wang, Y., et al. (2023). A two-stage optimal scheduling model of integrated energy system based on CVaR theory implementing integrated demand response. *Energy* 263, 125783. doi:10.1016/j.energy.2022.125783

Jiao, P. H., Chen, J. J., Cai, X., Wang, L., Zhao, Y., Zhang, X., et al. (2021). Joint active and reactive for allocation of renewable energy and energy storage under uncertain coupling. *Appl. Energy* 302, 117582. doi:10.1016/j.apenergy.2021.117582

Li, J. Y., Chen, J. J., Wang, Y. X., and Chen, W. (2024b). Combining multi-step reconfiguration with many-objective reduction as iterative bi-level scheduling for stochastic distribution network. *Energy* 290, 130198. doi:10.1016/j.energy.2023.130198

Li, Z., Pu, H., and Li, T. (2024a). Knowledge mapping and evolutionary analysis of energy storage resource management under renewable energy uncertainty: a bibliometric analysis. *Front. Energy Res.* 12, 1394318. doi:10.3389/fenrg.2024.1394318

Lin, Z., Wu, Q., Chen, H., Ji, T., Xu, Y., and Sun, H. (2023). Scenarios-oriented distributionally robust optimization for energy and reserve scheduling. *Ieee Trans. Power Syst.* 38 (3), 2943–2946. doi:10.1109/tpwrs.2023.3244018

Liu, J., Chen, J., Yan, G., Chen, W., and Xu, B. (2023). Clustering and dynamic recognition based auto-reservoir neural network: a wait-and-see approach for short-term park power load forecasting. *Iscience* 26 (8), 107456. doi:10.1016/j.isci.2023.107456

Lu, X., and Zhou, K. (2024). A distributionally robust optimization approach for optimal load dispatch of energy hub considering multiple energy storage units and demand response programs. *J. Energy Storage* 78, 110085. doi:10.1016/j.est.2023.110085

Ma, S., Liu, L., and Cheng, H. (2024). Power generation–network–load–energy storage co-planning under uncertainty. *Front. Energy Res.* 12, 1355047. doi:10.3389/fenrg.2024.1355047

Pan, Y., Zhu, M., Lv, Y., Yang, Y., Liang, Y., Yin, R., et al. (2023). Building energy simulation and its application for building performance optimization: a review of methods, tools, and case studies. *Adv. Appl. Energy* 10, 100135. doi:10.1016/j.adapen.2023.100135

Ren, C., Wei, Z., Zhou, Y., Chen, S., Han, H., Sun, G., et al. (2024). Distributionally robust CVaR optimization for resilient distribution system planning with consideration for long-term and short-term uncertainties. *Reliab. Eng. & Syst. Saf.* 251, 110378. doi:10.1016/j.ress.2024.110378

Skalyga, M., Amelin, M., Wu, Q., and Söder, L. (2023). Distributionally robust day-ahead combined heat and power plants scheduling with Wasserstein Metric. *Energy* 269, 126793. doi:10.1016/j.energy.2023.126793

Subbaramaiah, K., and Sujatha, P. (2023). Optimal DG unit placement in distribution networks by multi-objective whale optimization algorithm & its techno-economic analysis. *Electr. Power Syst. Res.* 214, 108869. doi:10.1016/j.epsr.2022.108869

Wang, C., Liu, C., Chen, J., and Zhang, G. (2024a). Cooperative planning of renewable energy generation and multi-timescale flexible resources in active distribution networks. *Appl. Energy* 356, 122429. doi:10.1016/j.apenergy.2023.122429

Wang, D., Zhang, C., Li, J., Zhu, L., Zhou, B., Zhou, Q., et al. (2024b). A novel interval power flow method based on hybrid box-ellipsoid uncertain sets. *IEEE Trans. Power Syst.* 39 (4), 6111–6114. doi:10.1109/tpwrs.2024.3391921

Wang, H., Shen, X., and Liu, J. (2022). Planning of new distribution network considering green power certificate trading and carbon emissions trading. *Energies* 15 (7), 2435. doi:10.3390/en15072435

Wang, Y. X., Chen, J. J., Zhao, Y. L., and Xu, B. (2024c). Incorporate robust optimization and demand defense for optimal planning of shared rental energy storage in multi-user industrial park. *Energy* 301, 131721. doi:10.1016/j.energy.2024.131721

Zhang, C., Liu, Q., Zhou, B., Chung, C. Y., Li, J., Zhu, L., et al. (2022). A central limit theorem-based method for DC and AC power flow analysis under interval uncertainty of renewable power generation. *IEEE Trans. Sustain. Energy* 14 (1), 563–575. doi:10.1109/tste.2022.3220567

Zhang, H., Wang, J., Zhao, X., and Yang, J. (2023b). Risk-assessment of carbon-dioxide recycling in a gas-fired power plant using CVaR-based convex optimization. *J. Clean. Prod.* 416, 137898. doi:10.1016/j.jclepro.2023.137898

Zhang, Q., Guo, Y., Wang, Z., and Bu, F. (2021). Distributed optimal conservation voltage reduction in integrated primary-secondary distribution systems. *IEEE Trans. Smart Grid* 12 (5), 3889–3900. doi:10.1109/tsg.2021.3088010

Zhang, Q., Yan, J., Gao, H. O., and You, F. (2023a). A systematic review on power systems planning and operations management with grid integration of transportation electrification at scale. *Adv. Appl. Energy* 11, 100147. doi:10.1016/j.adapen.2023.100147

Zhang, Y. Q., Chen, J. J., Wang, Y. X., and Feng, L. (2024). Enhancing resilience of agricultural microgrid through electricity–heat–water based multi-energy hub considering irradiation intensity uncertainty. *Renew. Energy* 220, 119739. doi:10.1016/j.renene.2023.119739

Zheng, F., Meng, X., Xu, T., Sun, Y., and Wang, H. (2023). Optimization method of energy storage configuration for distribution network with high proportion of photovoltaic based on source–load imbalance. *Sustainability* 15 (13), 10628. doi:10.3390/su151310628